β-delayed proton decays near the proton drip line

S.-W. Xu,* Z.-K. Li, Y.-X. Xie, Q.-Y. Pan, W.-X. Huang, X.-D. Wang, Y. Yu, and Y.-B. Xing
Institute of Modern Physics, Chinese Academy of Sciences, Lanzhou 730000, People's Republic of China

N.-C. Shu and Y.-S. Chen
China Institute of Atomic Energy, Beijing 102413, People's Republic of China

F.-R. Xu
Department of Technical Physics and MOE Key Laboratory, Peking University, Beijing 100871, People's Republic of China

K. Wang
Shanghai Institute for Nuclear Research, Shanghai 201800, People's Republic of China
(Received 22 September 2004; published 26 May 2005)

We briefly reviewed and summarized the experimental study on β-delayed proton decays published by our group over the last 8 years, namely the experimental observation of β-delayed proton decays of nine new nuclides in the rare-earth region near the proton drip line and five nuclides in the mass 90 region with $N \sim Z$ by utilizing the p-γ coincidence technique in combination with a He-jet tape transport system. In addition, important technical details of the experiments were provided. The experimental results were compared to the theoretical predictions of some nuclear models, resulting in the following conclusions. (1) The experimental half-lives for ^{85}Mo, ^{92}Rh, as well as the predicted "waiting point" nuclei ^{89}Ru and ^{93}Pd were 5–10 times longer than the macroscopic-microscopic model predictions of Möller *et al*. [At. Data Nucl. Data Tables **66**, 131 (1997)]. These data considerably influenced the predictions of the mass abundances of the nuclides produced in the *rp* process. (2) The experimental assignments of spin and parity for the drip-line nuclei ^{142}Ho and ^{128}Pm could not be well predicted by any of the nuclear models. Nevertheless, the configuration-constrained nuclear potential-energy surfaces calculated by means of a Woods-Saxon-Strutinsky method could reproduce the assignments. (3) The ALICE code overestimated by one or two orders of magnitude the production-reaction cross sections of the nine studied rare-earth nuclei, while the HIVAP code overestimated them by approximately one order of magnitude.

DOI: 10.1103/PhysRevC.71.054318 PACS number(s): 23.40.Hc, 21.10.Tg, 25.70.Gh, 27.60.+j

I. INTRODUCTION

Synthesis of the nuclei near the drip line and the study of their exotic decays deal with physics under extreme conditions because of the extreme limits of N/Z and therefore represent one of the frontiers of nuclear physics today. The rare-earth nuclei near the proton drip line have been predicted to be highly deformed [1]. They are the ideal objects for examining the correlations between nuclear deformation, pairing effects, and exotic decays. The proton drip line of odd-Z nuclei in the rare-earth region was speculated to be along the line $Z = 0.743N + 11.6$ in the chart of nuclides by Hofmann [2]. The proton activities near this line have been searched by different groups [3] for more than two decades. In the mass 90 region, the proton drip line is close to the $N = Z$ line as well as the reaction path of the *rp* process [4]. The β-delayed proton (βp) decays near the proton drip line in both rare-earth and mass 90 regions have been a major project studied by our group for nearly 10 years. The βp-decay process, which deals with proton emission from excited states, is related to proton activity from the ground state. It could provide important information on the structure of low-lying states and the production cross sections of nuclei near the proton drip line. One difference is that the spectra of proton radioactivity have discrete energy lines whereas the energy spectra of βp in the two regions are continuous. One difficulty encountered in examining the continuous-energy βp near the drip line is isobaric contamination. The unambiguous identification of a βp precursor requires mass separation and additional measurements, such as those of x-ray-proton coincidences, i.e., the coincidences between the characteristic x rays of the proton emitter and the βp. However, because of the low branching ratio of the electron capture (EC), the x-p coincidence measurements reduce the counting rate by one or two orders of magnitude. This fact severely constrains the study of a βp channel with the production cross section as low as 100 nb, and leads us to use a different technique to identify the βp precursor. In the EC/β^+ decay of an even(Z)-odd(N) βp precursor, some excited states in the even($Z-2$)-even($N+1$) daughter of each odd($Z-1$)-even($N+1$) proton "emitter" can be populated. The deexcitations from the excited states result in the transition between the lowest-energy 2^+ state and the 0^+ ground state in the daughter nucleus. Therefore, the coincidence between βp and the characteristic $2^+ \longrightarrow 0^+$ γ-ray transition for a particular daughter nucleus, a p-γ coincidence, can be used to identify the mother, the βp precursor. This method can also be used to identify some odd(Z)-odd(N) precursors. It should be noted that the sum

*Electronic address: XSW@NS.LZB.AC.CN

of the proton branching ratios ($b_{\beta p}$) to the excited states followed by the $2^+ \longrightarrow 0^+$ γ-ray transition in the daughter nucleus is larger than the EC branching ratio followed by βp emission. On the other hand, the transportation efficiency of a He-jet tape transport system (HJTTS) for the rare-earth or refractory nuclei is higher than the overall efficiency of an isotope separator on line (ISOL). Generally speaking, using the p-γ coincidence in combination with a HJTTS increases the efficiency of measuring the βp specific for a particular rare-earth or refractory nucleus by a factor of 50 compared to using the x-p coincidence in combination with an ISOL facility. Nine βp precursors [5–9] near the line $Z = 0.743N + 11.6$ in the rare-earth region [Fig. 1(a)] have been identified for the first time by our group using the p-γ coincidence, including predicted drip-line nuclei ^{142}Ho and ^{128}Pm. Moreover, new data on five refractory nuclei [10–12] in the mass 90 region near the $N = Z$ line [Fig. 1(b)] have been published by our group, including the predicted "waiting point" nuclei in the *rp* process, ^{89}Ru and ^{93}Pd. In this paper, some important technical details of the experiments are supplemented, and the experimental results are summarized and compared with the predictions of current nuclear models.

II. EXPERIMENTAL PROCEDURE

The experiments were carried out at the sector-focusing cyclotron in the Institute of Modern Physics, Lanzhou, China.

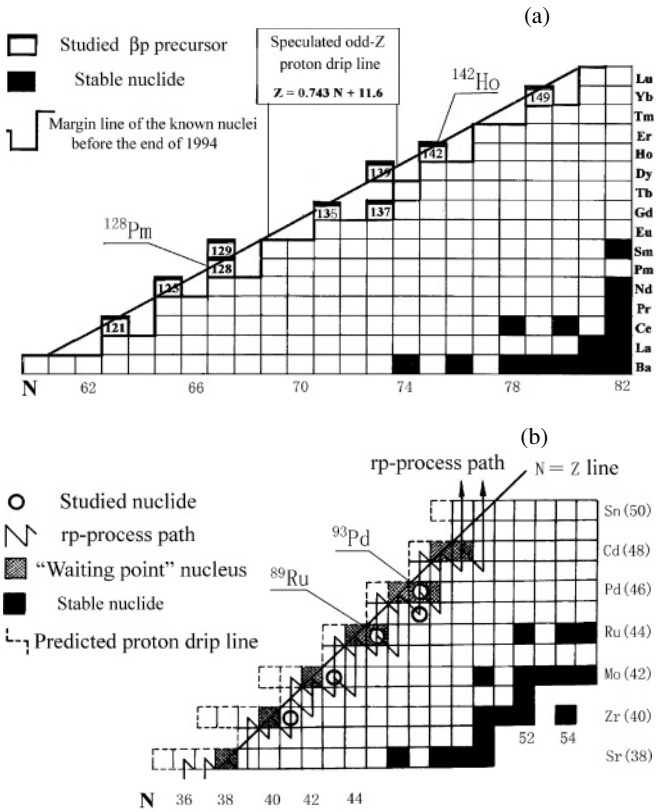

FIG. 1. (a) Rare-earth nuclides on the neutron deficient side; (b) nuclides in the mass 90 region near the $N = Z$ line.

Beams of ^{32}S, ^{36}Ar, or ^{40}Ca with the energies of 5–6 MeV/amu from the cyclotron entered a target chamber filled with 1-atm. helium, passing through a 1.89 mg/cm^2 thick Havar window, and finally bombarded a self-supporting metal target with a thickness of about 2.0 mg/cm^2, such as ^{92}Mo, ^{96}Ru, ^{106}Cd, or ^{112}Sn. Normally, the beam intensity was about 0.5 $e\,\mu$A. The studied nuclei were produced via fusion-evaporation reactions, for instance, $3n$-, $p3n$-, and $2p3n$-evaporation channels. The low melting-point targets ^{106}Cd and ^{112}Sn were mounted on a copper wheel that was surrounded by a cooling device and could be rotated. Reaction products recoiling out of the target foil thermalized in the helium gas and attached themselves to the aerosol clusters. NaCl or $PbCl_2$ were used as the aerosol at the temperature of 600° or 430°C, respectively. A He-jet (Fig. 2) then swept the clusters and reaction products through a Teflon capillary, 6.0 m long and 2 mm in diameter, and implanted them into a movable tape in a collection chamber. After a certain period of collection, the radioactivity on the tape was removed to a shielded counting room for p-γ_1(x)-γ_2(x)-t coincidence measurements. The sum of the thermalization time in the target chamber and the transportation time through the capillary for the reaction products T_t was estimated to be 0.1 s, and the tape-moving time of the system T_m was designed to be about 0.16 s. The lower limit of the half-life of the studied nuclei strongly depends on the sum of T_t and T_m. While the first activity sample was being counted, the next one was being collected. Usually, the collection time (or measuring time) was selected as the half-life of the studied nucleus multiplied by a factor of 2.2, so as to suppress activity from reaction products with shorter and longer half-lives. The transport efficiency of our HJTTS for the fission products of a ^{252}Cf source was tested and found to be 60–80%. Two 570 mm^2 $\times$ 350 μm totally depleted silicon surface barrier detectors used for the proton measurements were located on two opposite sides of the movable tape. Behind each silicon detector, a coaxial HpGe(GMX) detector measured γ(x) (Fig. 2). Energy and time spectra of γ(x) rays and protons were taken in coincidence mode. A personal computer controlled the HJTTS operations such as target rotation, activity collection, tape movement, start and stop of data acquisition, and so on.

III. IDENTIFICATION

The p-γ coincidence in combination with HJTTS was employed to identify the nuclei studied. For example, since the ground-state band of ^{120}Ba was already known [13], the 186 keV γ ray, namely the characteristic γ transition from the lowest-energy 2^+ state to the 0^+ ground state in the daughter ^{120}Ba, coincident with βp could be used to identify the precursor ^{121}Ce (Fig. 3). The nuclide ^{121}Ce was produced via the ^{92}Mo (^{32}S, $3n$) reaction. The decay γ spectrum from the products in the reaction of ^{32}S + ^{92}Mo gated on 2.5–6.0 MeV protons is shown in Fig. 4, where we have seen the characteristic 186 keV peak corresponding to the γ transition from $2^+ \longrightarrow 0^+$ in the daughter ^{120}Ba, and a small 358 keV peak corresponding to the γ transition from $4^+ \longrightarrow 2^+$ in ^{120}Ba.

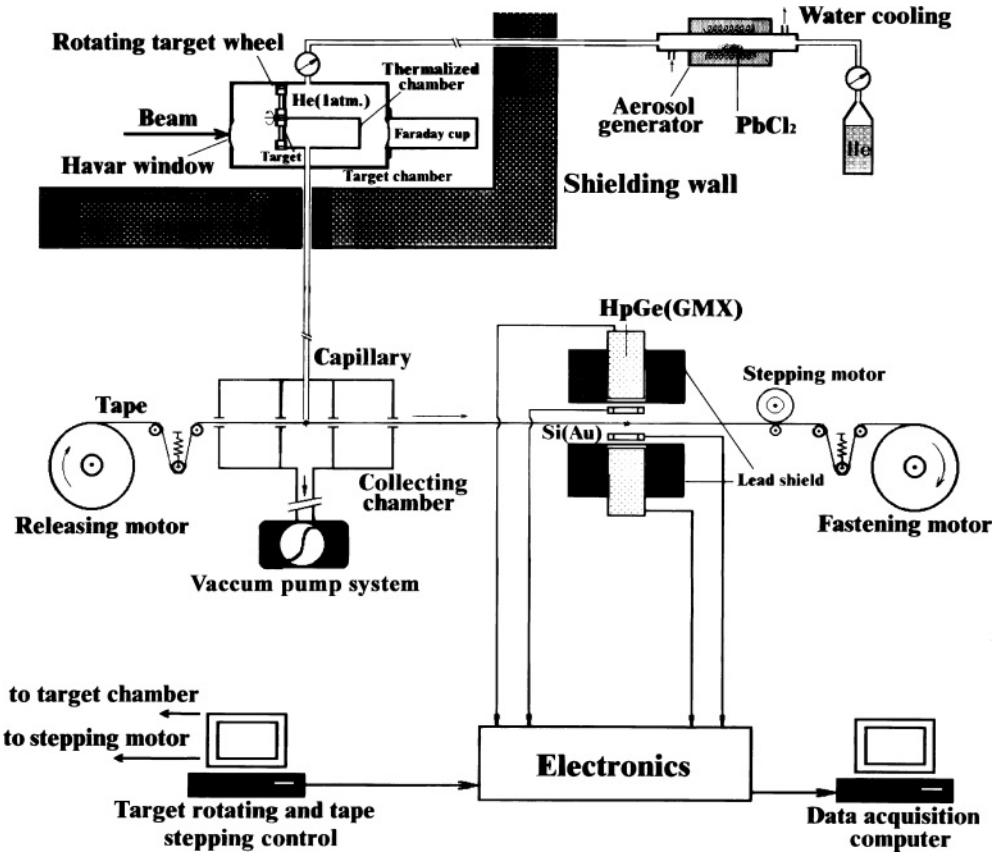

FIG. 2. Sketch of our experimental setup, including a target chamber, a He-jet tape transport system, and a counting room.

To confirm the identification, sometimes a triple coincidence was made. In the decay of ^{121}Ce, the x-ray spectrum gated on both the 2.5–6.0 MeV protons and the 186 keV γ ray is shown in Fig. 5, where we have seen a tiny peak with the central energy of 33.4 keV, which corresponds to the $K_{\alpha 1}$ x ray of La.

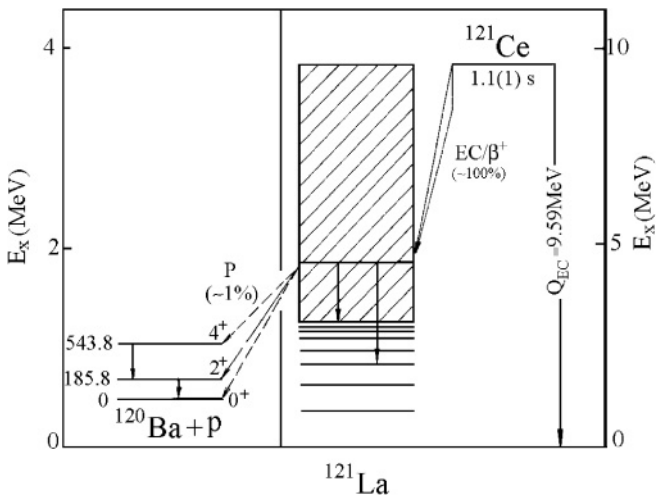

FIG. 3. Partial decay scheme for βp decay of ^{121}Ce.

IV. RESULTS AND DISCUSSION

A. Half-life

The experimental half-life of the studied precursor was extracted from the decay curve of the characteristic $2^+ \longrightarrow 0^+$ γ ray gated on β-delayed protons (Fig. 6). The experimental half-lives of the nine rare-earth nuclei together with the theoretical predictions of some nuclear models are listed in Table I. The experimental results are reasonably consistent with the predictions.

The experimental half-lives of the five nuclei studied in the mass 90 region near the $N = Z$ line together with the theoretical predictions of some nuclear models are listed in Table II. As shown in this table, the experimental values are 5–10 times greater than the predictions given by Möller *et al.* [17] with the exception of ^{81}Zr. The predicted nuclear properties in Ref. [17] have been used as the nuclear input data for astrophysics. The calculated abundances of the nuclides produced in the *rp* process will be changed considerably if our experimental half-lives are used as input data instead of the predictions given in [17]. To clearly analyze this influence, a network calculation was made for the time-integrated *rp*-process reaction flow during the x-ray burst at the typical conditions of temperature $T_9 = 1.5$ and density $\rho = 1.5 \times 10^6$ g/cm^3 [19]. The capture reaction rates, the photodisintegration rates and the β-decay half-lives are the main nuclear inputs for the *rp*-process network calculation.

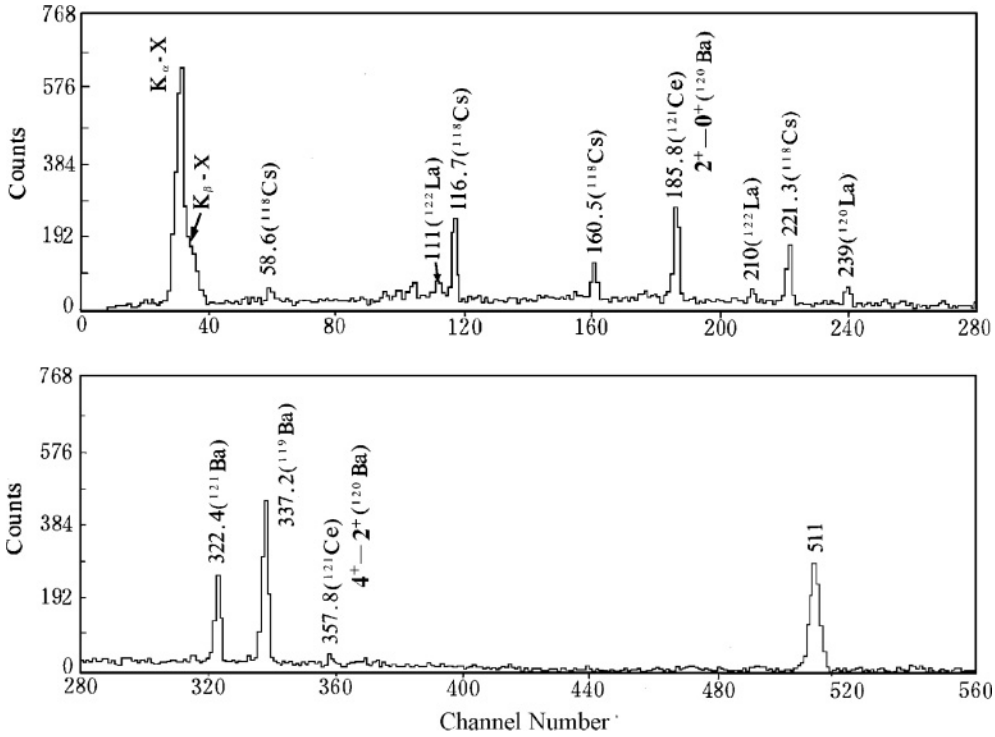

FIG. 4. Measured γ(x)-ray spectrum in coincidence with 2.5–6.5 MeV protons in the $^{32}S + ^{92}Mo$ reaction. The intense peaks are labeled with their energies in keV and their β -delayed proton precursors.

We employed two sets of the nuclear input data: the standard one taken from Schatz *et al*. [4] and the present set in which our experimental β-decay half-lives for the four nuclei ^{93}Pd, ^{92}Rh, ^{89}Ru, and ^{85}Mo were used to replace those in the standard data set. The only difference between these two data sets is that they have different half-lives for the four nuclei. Those in the standard set are originally quoted from the theoretical predictions in Ref. [17]. The nuclear reaction network included all proton-rich nuclei from hydrogen to the isotopes above the $A = 100$ region. Helium burns mainly via the triple-α reaction and the αp process, a sequence of alternating (α, p) and (p, γ) reactions into the $A = 60$ region. The seed nuclei for the *rp* process are provided by these helium burning processes. Along the reaction path of the *rp* process, waiting point nuclei play a particularly important role in controlling the process. At a waiting point nucleus, the Q value of the (p, γ) reaction is small or negative, so that the photodisintegration could restrain the occurrence of the (p, γ) reaction, and the nucleus has to wait for the β decay to continue the process. The waiting point nuclei will store the produced material until the burning is over. Therefore, the longer-lived waiting point nuclei along the reaction path will store more material at the end of the *rp* process. The detailed analysis of the calculated reaction flux patterns suggested some waiting

TABLE I. Half-lives of the nine rare-earth nuclei studied.

Nuclide	Measured half-life (s)	Theoretical predictions (s)				
		Gross theory [14,15]	Microscopic theory		[16]	Möller *et al*. [17]
			Hilf	Groote	Möller	
^{121}Ce	1.1 ± 0.1	0.4–1.5	1.29	1.51	1.04	0.91
^{125}Nd	0.65 ± 0.15	0.67	0.79	0.78	0.58	0.42
^{128}Pm	1.0 ± 0.3	0.71	1.80	2.5	1.5	0.40
^{129}Sm	0.55 ± 0.10	0.58	0.33	–	–	0.20
^{135}Gd	1.1 ± 0.2	0.3–1.5	–	0.62	1.1	0.69
^{137}Gd	2.2 ± 0.2	1–3	1.1	1.7	–	2.0
^{139}Dy	0.6 ± 0.2	0.61	–		0.47	0.50
^{142}Ho	0.4 ± 0.1	0.44	0.57	0.65	0.64	0.44
^{149}Yb	0.7 ± 0.2	0.75	0.72	1.2		0.30

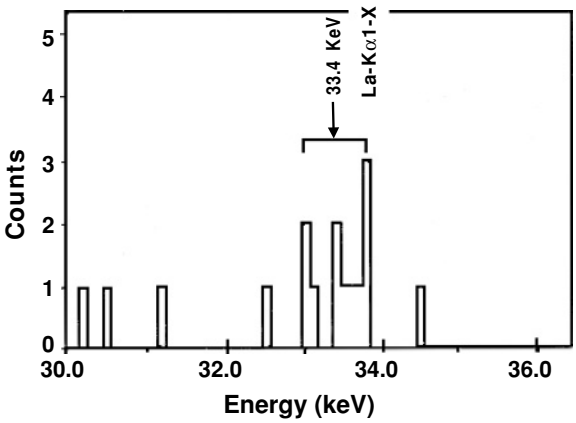

FIG. 5. Observed x spectrum gated on both 2.5–6.0 MeV protons and the 186 keV γ ray in the $^{32}S + ^{92}Mo$ reaction.

point nuclei in the $A = 80 - 100$ region, ^{80}Zr, ^{84}Mo, ^{88,89}Ru, ^{92,93}Pd, and ^{96}Cd. To make a comparison, the abundances of the waiting point nuclei ^{89}Ru and ^{93}Pd as functions of the processing time were calculated with both the present set of the nuclear input data and the standard set, and shown in Fig. 7. It can be seen that the calculated abundances of ^{89}Ru and ^{93}Pd with the present experimental half-lives are larger than those with the standard predicted half-lives during the entire processing time, and the present experimental half-lives lead to about 4 times the yield of these two waiting point nuclei around the peak abundances.

B. Spin, parity, and deformation

The experimental values for the spins and parities were extracted by fitting the measured βp energy spectrum and relative βp branching ratios ($b_{\beta p}$) to low-lying states in the daughter nucleus with a statistical model calculation [20]. For example, the measured βp energy spectrum of ^{121}Ce fitted by the statistical model calculation with the initial spins and parities $5/2^+$ and $5/2^-$ is shown in Fig. 8. Both calculated spectra fit the experimental result equally well. On the other hand, if the spin and parity of ^{121}Ce are assumed to be $5/2^+$ and $5/2^-$, the calculated ratios of $b_{\beta p}(4^+)/b_{\beta p}(2^+)$ of ^{120}Ba would be 27% and 20%, respectively. Both of them are consistent with the experimental ratio $19 \pm 9\%$, while other spin and/or parity assumptions give relative βp branching ratios that are at variance with the experiment. Finally, $5/2^+$ or $5/2^-$ were assigned to the spin and parity of the ground state of ^{121}Ce.

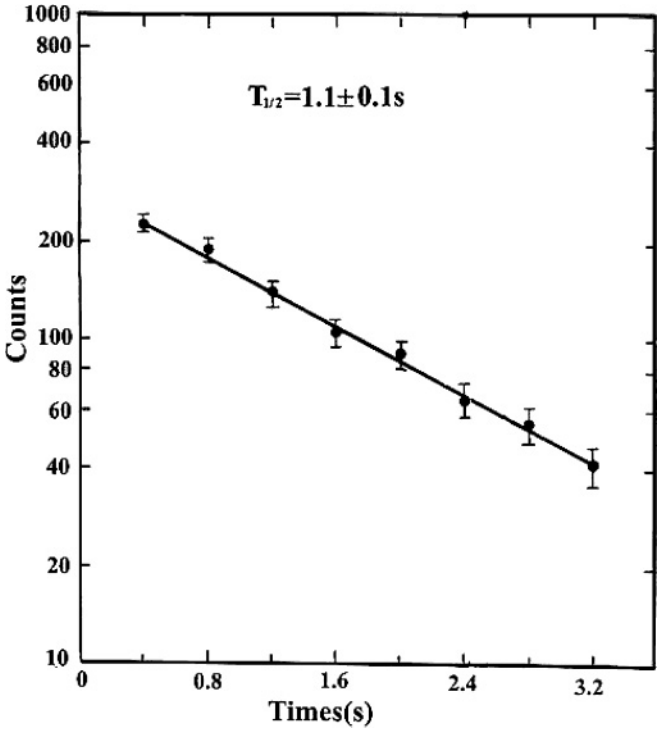

FIG. 6. Decay curve of the characteristic 186 keV γ ray gated on β-delayed protons for the products in the $^{32}S + ^{92}Mo$ reaction. The half-live of the precursor ^{121}Ce was extracted to be 1.1 ± 0.1 s.

The experimental spins and parities of the nine rare-earth nuclei are listed in Table III and compared with the theoretical predictions of some nuclear models. It can be seen that the experimental spin-parity values of the seven even(Z)-odd(N) nuclei in Table III are in reasonable agreement with theoretical predictions. The theoretical determination of the ground-state spin and parity for an even-odd nucleus based on the orbital occupied by the last neutron in the Nilsson diagram strongly depends on the nuclear deformation. Therefore, the consistency between the experimental spin-parity assignments and the predicted Nilsson diagrams in Refs. [17,21,22] is an indirect indication that the six even-odd nuclei ^{121}Ce, ^{125}Nd, ^{129}Sm, ^{135}Gd, ^{137}Gd, and ^{139}Dy are highly deformed with $\beta_2 \sim 0.3$ in the spherical-harmonic expansion. However, the experimental spin-parity assignments of the odd-odd nuclei ^{142}Ho and ^{128}Pm are not in good agreement

TABLE II. Half-lives of the five nuclei studied in the mass 90 region near the $N = Z$ line.

Nuclide	Measured half-life (s)	Theoretical predictions (s)			
		Gross theory [14,15]	Herndl & Brown [18]	Microscopic [16]	Möller *et al.* [17]
^{81}Zr	5.3 ± 0.5	0.7–5.0	–	–	4.3
^{85}Mo	3.2 ± 0.2	0.5–3.0	–	–	0.37
^{89}Ru	1.2 ± 0.2	3.8	4.0	0.43–0.89	0.29
^{92}Rh	3.0 ± 0.8	1.1	4.3	–	0.35
^{93}Pd	1.3 ± 0.2	0.2–1.0	1.4	0.25–0.58	0.22

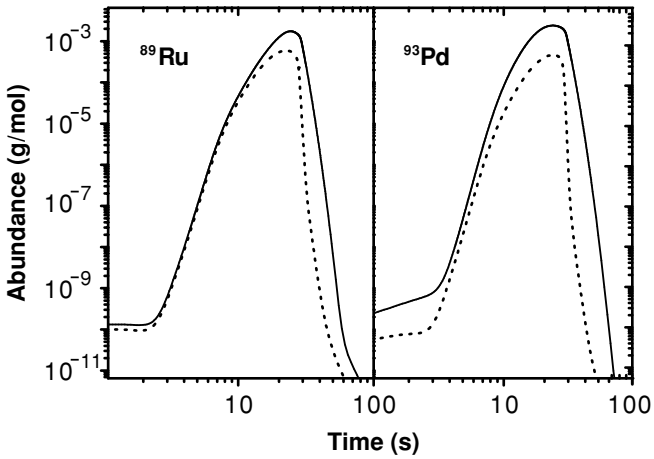

FIG. 7. Calculated abundances of ^{89}Ru and ^{93}Pd as functions of the processing time for the *rp* process at the typical conditions of the x-ray bursts, $T_9 = 1.5$ and $\rho = 1.5 \times 10^6$ g/cm^3. The dotted curve represents the results when the standard set of nuclear input data was used in the network calculations; the solid curve represents the results when the experimental half-lives of ^{85}Mo, ^{89}Ru, ^{92}Rh, and ^{93}Pd were used in the input data instead and the rest of the input data were the same as those in the standard set.

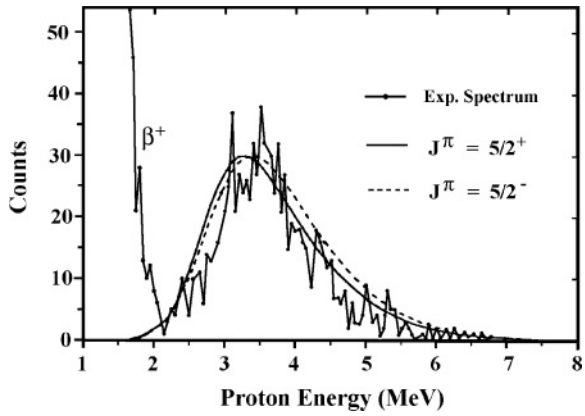

FIG. 8. The energy spectrum of βp gated by the 186 keV γ ray in the ^{32}S + ^{92}Mo reaction. Solid and dotted curves were calculated by using the statistical model with two different initial spins and parities of ^{121}Ce.

with any theoretical predictions in Table III. Recently, the configuration-constrained potential-energy surfaces (PES) for the two odd-odd nuclei were calculated by using a Woods-Saxon-Strutinsky method [24]. In the calculated PES for the negative-parity configuration of ^{142}Ho [Fig. 9(a)], a minimum with $\beta_2 = 0.251$ and $\gamma = 9.3^\circ$ was found, which corresponds to the configuration of $(\pi 7/2^-[523] \times \nu 7/2^+[404])\ 7^-$; while in the calculated PES for the positive-parity configuration of ^{128}Pm [Fig. 9(b)], a minimum with $\beta_2 = 0.319$ and $\gamma = -0.8^\circ$ was found, which corresponds to the configuration of $(\pi 5/2^-[532] \times \nu 7/2^-[523])\ 6^+$. The calculated PES gives 7^- for ^{142}Ho and 6^+ for ^{128}Pm in good agreement with our experimental spin-parity assignments, and indicates that ^{142}Ho and ^{128}Pm also are highly deformed with $\beta_2 \sim 0.3$.

The experimental spin-parity assignments of the five nuclei in the mass 90 region with $N \sim Z$ compared with the theoretical predictions of some nuclear models are listed in Table IV. Note that the experimental spin-parity of ^{85}Mo, $1/2^+$, is not consistent with any predictions in Table IV. The inconsistency, most probably, is because nuclear deformation near ^{85}Mo varies dramatically; therefore, its spin-parity is not easily reproduced by any model calculations.

C. Production cross section

According to the measured counting rate of βp, the production cross sections for the nine rare-earth nuclei were estimated and are listed in Table V. The $\sigma_{\beta p}$ in column 4 of Table V is the fractional cross section of the βp-decay channel with the uncertainty of a factor of 2. Uncertainty brought from the calculation of the branching ratio of βp should be taken into account. Finally, the experimental fusion-evaporation reaction cross section was estimated with an uncertainty of a factor of 3. On the other hand, the fusion-evaporation reaction cross section ($\sigma_{\rm fe}$) was calculated by using ALICE [25] and HIVAP [26] codes with normal input parameters. The calculated reaction cross sections also are listed in Table V. Typically, the ALICE

TABLE III. Spins and parities for the nine neutron deficient rare-earth nuclei.

Nuclide	Spin and Parity					Deformation ε_2 [1]
		Theoretical predictions				
	Experimental value	Arseniev *et al.* [21]	Bengtsson *et al.* [22]	Audi *et al.* [23]	Möller *et al.* [17]	
^{121}Ce	$5/2^\pm$	$5/2^+$	$5/2^-$	$5/2^+$	$3/2^+$	0.29
^{125}Nd	$5/2^\pm$	$5/2^+$	$5/2^+$		$5/2^+$	0.30
^{128}Pm	$5^\pm, 6^\pm, 7^\pm$		3^-		3^-	0.30
^{129}Sm	$1/2^+, 3/2^+$	$1/2^+$	$1/2^+$		$1/2^+$	0.30
^{135}Gd	$5/2^+$	$5/2^+$	$5/2^+$	$5/2^+$	$5/2^+$	0.28
^{137}Gd	$7/2^\pm$	$7/2^+$	$7/2^+, 1/2^+$	$7/2^+$	$9/2^-$	0.27
^{139}Dy	$7/2^+$	$7/2^+$	$7/2^+$	$7/2^+$	$9/2^+$	0.26
^{142}Ho	$5^\pm, 6^\pm, 7^\pm$	$5^-, 8^+$	8^+		8^+	0.25
^{149}Yb	$1/2^\pm$	$1/2^-$	$1/2^-$	$1/2^+, 3/2^+$	$1/2^-$	−0.16

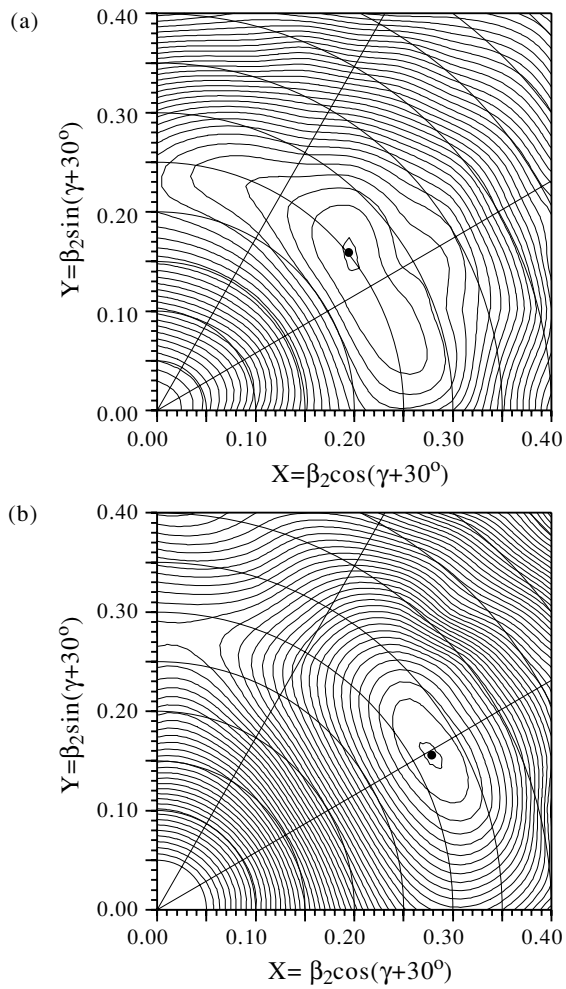

FIG. 9. Calculated potential-energy surfaces of (a) ^{142}Ho for the negative-parity configurations and (b) ^{128}Pm for the positive-parity configurations.

code overestimates the $\sigma_{\rm fe}$ by one or two orders of magnitude, while the HIVAP code overestimates it by approximately one order of magnitude.

V. SUMMARY

The p-γ coincidence is an effective but simple method of studying the βp decays near the proton drip line, in particular, for the even-odd precursors. Generally speaking, using the p-γ coincidence in combination with a HJTTS system, the efficiency of measuring βp specifically for a particular rare-earth or refractory precursor can be increased by a factor of 50 in comparison with that using the x-p coincidence in combination with an ISOL facility. By using the p-γ coincidence, we identified for the first time, nine βp precursors in the rare-earth region near the proton drip line with the cross sections of βp channel from 50 to 450 nb, including the predicted drip-line nuclei ^{142}Ho and ^{128}Pm. We also obtained new data on βp decays for five refractory nuclei with $N \sim Z$ in the mass 90 region using the same technique, including the important data for the predicted waiting point nuclei in the *rp* process, ^{89}Ru and ^{93}Pd.

The half-lives of the rare-earth nuclei near the line $Z = 0.743N + 11.6$ were measured to be about 1 s, which are in reasonable agreement with the theoretical predictions of some nuclear models, while the measured half-lives of ^{85}Mo, ^{89}Ru, ^{92}Rh, and ^{93}Pd are 5–10 times longer than the theoretical predictions given by Möller *et al*. [17]. The latter are usually used as the nuclear input data for astrophysics. The abundances of the waiting point nuclei ^{89}Ru and ^{93}Pd as functions of the processing time for the *rp* process at typical conditions of x-ray bursts were obtained by a network calculation, which showed that such lengthening of the half-lives of the four nuclei leads to about 4 times more products of these two waiting point nuclei around the peak abundances.

The extracted spins and parities of the studied βp precursors by fitting the βp energy spectra and branching ratios within the framework of a statistical model are in reasonable agreement with the theoretical predictions of some nuclear models, except those of ^{142}Ho, ^{128}Pm, and ^{85}Mo. However, the calculated configuration-constrained PES for the odd-odd nuclei ^{142}Ho and ^{128}Pm by using the Woods-Saxon-Strutinsky method reproduced the experimental assignments. As expected, the studied rare-earth nuclei, except ^{149}Yb, are highly deformed with $\beta_2 \sim 0.3$. Possibly, because the shape of the nucleus near ^{85}Mo varies dramatically, the extracted spin and parity of ^{85}Mo could not be reproduced by any model calculations.

Based on the counting rate of β-delayed protons, the $\sigma_{\rm fe}$ for producing the nine rare-earth precursors were estimated and compared with calculated results by using ALICE and HIVAP codes, respectively. On the average, the ALICE code

TABLE IV. Spins and parities for the five nuclei in the mass 90 region with $N \sim Z$.

Nuclide	Spin and Parity					Deformation ε_2 [1]
		Theoretical predictions				
	Experimental value	Arseniev *et al*. [21]	Bengtsson *et al*. [22]	Audi *et al*. [23]	Möller *et al*. [17]	
^{81}Zr	$3/2^-$		$3/2^-$	$3/2^-$	$1/2^+$	0.40
^{85}Mo	$1/2^+$		$3/2^+$	$3/2^+$	$9/2^+$	0.05
^{89}Ru	$5/2^+, 7/2^\pm$	$9/2^+$	$5/2^+$	$5/2^+$	5/2	0.05
^{92}Rh	$9/2^\pm$	$9/2^+$	$7/2^+$	$9/2^+$	$7/2^+$	0.05
^{93}Pd	$\geqslant 5$	2^+	6^+	6^+	6^+	0.05

TABLE V. The fusion-evaporation reaction cross sections σ_{fe} for producing the nine rare-earth nuclei. The $\sigma_{\beta p}$ in column 4 stands for the reaction cross section of the βp channel, the $b_{\beta p}$ in column 5 is the branching ratio of βp decay.

Nuclide	Production reaction	Incident energy (MeV)	$\sigma_{\beta p}$(nb)	$b_{\beta p}$(%)	$\sigma_{fe}(\mu b)$		
					Experimental stimation[a]	ALICE [25]	HIVAP [26]
^{121}Ce	$^{32}S + ^{92}Mo$	151	250	12	2.1	146	27
^{125}Nd	$^{36}Ar + ^{92}Mo$	169	230	14	1.6	45	7.9
^{128}Pm	$^{36}Ar + ^{96}Ru$	174	50	6	0.8	54	47
^{129}Sm	$^{36}Ar + ^{96}Ru$	165	70	34	0.2	10	2.4
^{135}Gd	$^{32}S + ^{106}Cd$	151	100	18	0.6	142	23
^{137}Gd	$^{36}Ar + ^{106}Cd$	176	450	2	22.5	1770	93
^{139}Dy	$^{36}Ar + ^{106}Cd$	176	160	11	1.5	90	12
^{142}Ho	$^{40}Ca + ^{106}Cd$	202	85	7	1.2	109	64
^{149}Yb	$^{40}Ca + ^{112}Sn$	185	200	6	3.3	47	17

[a]The uncertainty is a factor of 3.

overestimates the σ_{fe} by one or two orders of magnitude; the HIVAP code overestimates it by approximately one order of magnitude. Obviously, the overestimation cannot be explained with our experimental error bar. Determining the reason for the overestimation is still an open problem.

ACKNOWLEDGMENTS

This work was supported by the National Natural Science Foundation of China (10375078 and 10475002) and the Major State Basic Research Development Program (G2000077402).

[1] P. Möller, J. R. Nix, W. D. Myers, and W. J. Swiatecki, At. Data Nucl. Data Tables **59**, 185 (1995).
[2] S. Hofmann, Radiochim. Acta **70/71**, 93 (1995).
[3] A. A. Sonzogni, Nucl. Data Sheets **95**, 1 (2002).
[4] H. Schatz, A. Aprahamina, J. Görres, M. Wiescher, T. Rauscher, J. F. Rembges, F.-K. Thielemann, B. Pfeiffer, P. Möller, K.-L. Kratz, H. Herndl, B. A. Brown, and H. Rebel, Phys. Rep. **294**, 167 (1998).
[5] Xu Shuwei, Xie Yuanxiang, and Li Zhankui *et al*., Z. Phys. A **356**, 227 (1996).
[6] Li Zhankui, Xu Shuwei, Xie Yuanxiang, Ma Ruichang, Ge Yuanxiu, Wang Chunfang, Huang Wenxue, and Zhang Tianmei, Phys. Rev. C **56**, 1157 (1997).
[7] S.-W. Xu, Z.-K. Li, Y.-X. Xie, Q.-Y. Pan, Y. Yu, J. Adam, C.-F. Wang, J.-P. Xing, Q.-Y. Hu, S.-H. Li, H.-Y. Chen, T.-M. Zhang, G.-M. Jin, Y.-X. Luo, Yu. Penionzhkevich, and Yu. Gangrsky, Phys. Rev. C **60**, 061302(R) (1999).
[8] S.-W. Xu, Z.-K. Li, Y.-X. Xie, X.-D. Wang, B. Guo, C.-G. Leng, Y. Yu, C.-F. Wang, J.-P. Xing, H.-Y. Chen, and T.-M. Zhang, Phys. Rev. C **64**, 017301 (2001).
[9] S.-W. Xu, Z.-K. Li, Y.-X. Xie, X.-D. Wang, B. Guo, C.-G. Leng, and Y. Yu, Eur. Phys. J. A **12**, 1 (2001).
[10] W.-X. Huang, R.-C. Ma, S.-W. Xu, X.-J. Xu, J.-S. Guo, X.-F. Sun, Y.-X. Xie, Z.-K. Li, Y.-X. Ge, Y.-Y. Wang, C.-F. Wang, T.-M. Zhang, G.-M. Jin, and Y.-X. Luo, Phys. Rev. C **59**, 2402 (1999).
[11] Li Zhankui, Xu Shuwei, and Xie Yuanxiang *et al*., Eur. Phys. J. A **5**, 351 (1999).
[12] S.-W. Xu, Z.-K. Li, Y.-X. Xie, X.-D. Wang, B. Guo, C.-G. Leng, and Y. Yu, Eur. Phys. J. A **11**, 375 (2001).
[13] B. Cederwall, A. Johnson, R. Wyss, F. Lidèn, B. Fant, S. Juutinen, P. Ahonen, J. Mukai, and J. Nyberg, Z. Phys. A **338**, 461 (1991).
[14] K. Takahashi, M. Yamada, and T. Kondoh, At. Data Nucl. Data Tables **12**, 101 (1973); S. I. Koyama, K. Takahashi, and M. Yamada, Prog. Theor. Phys. **44**, 663 (1970).
[15] T. Horiguchi, T. Tachibana, and J. Katakura, Chart of the Nuclides 2000. Japanese Data Committee and Nuclear Data Center, 2000 (unpublished).
[16] M. Hirsch, A. Staudt, K. Muto, and H. V. Klapdor-Kleingrothaus, At. Data Nucl. Data Tables **53**, 165 (1993).
[17] P. Möller, J. R. Nix, and K.-L. Kratz, At. Data Nucl. Data Tables **66**, 131 (1997).
[18] H. Herndl and B. A. Brown, Nucl. Phys. **A627**, 35 (1997).
[19] R. K. Wallace and S. E. Woosley, Astrophys. J. (Suppl.) **389**, 45 (1981).
[20] E. Hagberg, J. C. Hardy, H. Schmeing, E. T. H. Clifford, and V. T. Koslowsky, Nucl. Phys. **A395**, 152 (1983).
[21] D. A. Arseniev, A. Sobiczewski, and V. G. Solview, Nucl. Phys. **A126**, 15 (1969).
[22] T. Bengtsson and I. Ragnarsson, Nucl. Phys. **A436**, 14 (1985); R. B. Firestone, ed., *Table of Isotopes*, 8th ed. (Wiley, New York, 1996), Vol. II, App. H, H-7, and H-8.
[23] G. Audi, O. Bersillon, J. Blachot, and A. H. Wapstra, Nucl. Phys. **A624**, 1 (1997).
[24] W. Nazarewicz, J. Dudek, R. Bengtsson, T. Bengtsson, and I. Ragnarsson, Nucl. Phys. **A435**, 397 (1985).
[25] W. G. Winn, H. H. Gutbrod, and M. Blann, Nucl. Phys. **A188**, 423 (1987).
[26] W. Reisdorf, Z. Phys. A **300**, 227 (1981); M. Veselsky *et al*., *ibid.* **356**, 403 (1997).